jove

Translaminar Autonomous System Model for the Modulation of Intraocular and Intracranial Pressure in Human Donor Posterior Segments

Tasneem P. Sharma[1], **Stacy M. Curry**[1], **Husain Lohawala**[2], **Colleen McDowell**[3]

[1] North Texas Eye Research Institute, Department of Pharmacology and Neuroscience, University of North Texas Health Science Center [2] Mechanical Engineer Consultant [3] Department of Ophthalmology and Visual Sciences, School of Medicine and Public Health, University of Wisconsin

Corresponding Authors

Tasneem P. Sharma
tpsharma@iu.edu

Colleen McDowell
cmmcdowell@wisc.edu

Citation

Sharma, T.P., Curry, S.M., Lohawala, H., McDowell, C. Translaminar Autonomous System Model for the Modulation of Intraocular and Intracranial Pressure in Human Donor Posterior Segments. *J. Vis. Exp.* (158), e61006, doi:10.3791/61006 (2020).

Date Published

April 24, 2020

DOI

10.3791/61006

URL

jove.com/video/61006

Abstract

There is a current unmet need for a new preclinical human model that can target disease etiology ex vivo using intracranial pressure (ICP) and intraocular pressure (IOP) which can identify various pathogenic paradigms related to the glaucoma pathogenesis. Ex vivo human anterior segment perfusion organ culture models have previously been successfully utilized and applied as effective technologies for the discovery of glaucoma pathogenesis and testing of therapeutics. Preclinical drug screening and research performed on ex vivo human organ systems can be more translatable to clinical research. This article describes in detail the generation and operation of a novel ex vivo human translaminar pressure model called the translaminar autonomous system (TAS). The TAS model can independently regulate ICP and IOP using human donor posterior segments. The model allows for studying pathogenesis in a preclinical manner. It can reduce the use of living animals in ophthalmic research. In contrast to in vitro experimental models, optic nerve head (ONH) tissue structure, complexity, and integrity can also be maintained within the ex vivo TAS model.

Introduction

Global estimates in recent surveys suggest that 285 million people live with visual impairment, including 39 million who are blind[1]. In 2010, the World Health Organization documented that three of the nine listed leading causes of blindness occur in the posterior segment of the eye[1]. Posterior segment eye diseases involve the retina, choroid, and optic nerve[2]. The retina and optic nerve are central nervous system (CNS) extensions of the brain. The retinal ganglion cell (RGC) axons are vulnerable to damage because they exit the eye through the optic nerve head (ONH) to form the optic nerve[3]. The ONH remains the most vulnerable point for the RGC axons because of the 3D

meshwork of connective tissue beams called the lamina cribrosa (LC)[4]. The ONH is the initial site of insult to RGC axons in glaucoma[5,6,7], and gene expression changes within the ONH have been studied in ocular hypertension and glaucoma models[8,9,10]. The RGC axons are susceptible at the ONH due to pressure differentials between the intraocular compartment, called the intraocular pressure (IOP), and within the external perioptic subarachnoid space, called the intracranial pressure (ICP)[11]. The LC region separates both areas, maintaining normal pressure differentials, with IOP ranging from 10–21 mmHg and ICP from 5–15 mmHg[12]. The pressure difference through the lamina between the two chambers is called the translaminar pressure gradient (TLPG)[13]. A major risk factor of glaucoma is elevated IOP[14].

Increased IOP increases the strain within and across the laminar region[6,15,16]. Experimental observations in humans and animal models present the ONH as being the initial site of axonal damage[17,18]. The biomechanical paradigm of IOP-related stress and strain causing glaucomatous damage at the ONH also influences the pathophysiology of glaucoma[19,20,21]. Even though in humans pressure-induced changes mechanically damage RGC axons[22], rodents lacking collagenous plates within the lamina can also develop glaucoma[7,23]. In addition, elevated IOP remains the most prominent risk factor in primary open angle glaucoma patients, while normal tension glaucoma patients develop glaucomatous optic neuropathy even without elevated IOP. Furthermore, there are also a subset of ocular hypertensive patients that show no optic nerve damage. It has also been suggested that cerebrospinal fluid pressure (CSFp) may play a role in glaucoma pathogenesis. Evidence indicates that ICP is lowered to ~5 mmHg in glaucoma patients compared to normal individuals, thereby causing increased translaminar pressure and playing a crucial role in disease[24,25]. Previously, it was demonstrated in a canine model, that by controlling IOP and CSFp changes, there can be large displacements of the optic disc[26]. Elevating CSFp in porcine eyes has also shown increased principal strain within the LC region and retrolaminar neural tissue. Increased strain on the RGCs and the LC region contributes to axonal transport blockage and loss of RGCs[27]. Progressive degeneration of RGCs has been associated with loss of trophic support[28,29], stimulation of inflammatory processes/immune regulation[30,31], and apoptotic effectors[29,32,33,34,35]. Additionally, axonal injury (**Figure 3**) causes detrimental effects on the RGCs, triggering regenerative failure[36,37,38,39]. Even though the effects of IOP have been well studied, minimal research has been performed on abnormal translaminar pressure changes. Most treatments for glaucoma focus on stabilizing IOP. However, even though lowering of IOP slows the progression of the disease, it does not reverse visual field loss and prevent complete loss of RGCs. Understanding pressure-related neurodegenerative changes in glaucoma will be crucial to preventing RGC death.

Current evidence indicates that translaminar pressure modulations due to various mechanical, biological, or physiological changes in patients suffering from traumatic or neurodegenerative visual impairments can cause significant vision loss. Currently, no true preclinical human posterior segment model exists that can allow the study of glaucomatous biomechanical damage within the ex vivo human ONH. Observation and treatment of the posterior segment of the eye is a huge challenge in ophthalmology[27]. There are physical and biological barriers to target the posterior eye, including high elimination rates, blood-retinal barrier, and potential immunological responses[40]. Most efficacy and safety tests for novel drug targets are

accomplished utilizing in vitro cellular and in vivo animal models[41]. Ocular anatomy is complex, and in vitro studies do not accurately mimic the anatomical and physiological barriers presented by tissue model systems. Even though animal models are a necessity for pharmacokinetic studies, the ocular physiology of the human posterior eye may vary between various animal species, including cellular anatomy of the retina, vasculature, and ONH[41,42].

The use of living animals requires intensive and detailed ethical regulations, high financial commitment, and effective reproducibility[43]. Recently, multiple other guidelines have ensued for the ethical use of animals in experimental research[44,45,46]. An alternative to animal testing is the use of ex vivo human eye models to investigate disease pathogenesis and potential analysis of drugs for protecting ONH damage. Human postmortem tissue is a valuable resource for studying human disease paradigms, especially in the case of human neurodegenerative diseases, because identification of potential drugs developed in animal models require the need to be translatable to humans[47]. The ex vivo human donor tissue has been extensively utilized for the study of human disorders[47,48,49], and human anterior segment perfusion organ culture systems have previously provided a unique ex vivo model to study the pathophysiology of elevated IOP[50,51,52].

To study translaminar pressure related to IOP and ICP in human eyes, we successfully designed and developed a two-chamber translaminar autonomous system (TAS) that can independently regulate IOP and ICP using posterior segments from human donor eyes. It is the first ex vivo human model to study translaminar pressure and exploit the biomechanical effects of TLPG on the ONH.

This ex vivo human TAS model can be used to discover and classify cellular and functional modifications that occur due to chronic elevation of IOP or ICP. In this report, we detail the step-by-step protocol of dissecting, setting up, and monitoring the TAS human posterior segment model. The protocol will allow other researchers to effectively reproduce this novel ex vivo pressurized human posterior segment model to study biomechanical disease pathogenesis.

Protocol

Eyes were obtained according to the provisions of the Declaration of Helsinki for research involving human tissue.

NOTE: Eyes from reputable eye banks (e.g., Lions Eye Institute for Transplant, Research, Tampa FL) were harvested within 6–12 h of death and donor serum was tested for hepatitis B, hepatitis C, and human immunodeficiency virus 1 and 2. Once they were received, the eyes were dissected and set up in the TAS model within 24 h. Exclusion criteria included any ocular pathology. Eyes were not excluded based on age, race, or gender. To ensure the viability of the retina upon receipt, retinal explants were harvested from the tissue donors and cultured for 7 and 14 days (**Supplemental Figure 1**). These retinas were also dissociated and grew healthy RGCs in culture for 7 days with positive staining for RGC marker, RNA-binding protein with multiple splicing (RBPMS), as well as positive neurofilament light chain (NEFL) staining in their neurofilaments (**Supplemental Figure 2**). .

1. Preparation and sterilization of equipment and supplies

1. Refer to the **Table of Materials** for a complete list of supplies required as well as supplier and catalogue numbers.

2. Prior to use, sterilize all equipment and instruments by autoclaving or using ethylene oxide ampules.

2. Preparation of perfusion medium

1. Add 1% penicillin streptomycin (10,000 U/mL penicillin, 10,000 µg/mL streptomycin in 0.85% NaCl) and 1% L-glutamine (200 mM) to 1,000 mL high glucose Dulbecco's modified Eagle's medium (DMEM).
2. Sterilize the perfusion medium by passing through a 0.22 µm filter.

3. Translaminar autonomous system (TAS) setup

1. Set up inflow syringes (IOP and ICP reservoirs).
    1. Add 30 mL of the perfusion medium (section 2) to a 30 mL syringe. Attach a 3-way stopcock to the 30 mL syringe. Attach a 0.22 µm hydrophilic filter to the 3-way stopcock. Attach a 15 G Luer stub adapter to the 0.22 µm hydrophilic filter.
    2. Remove air bubbles from the syringe setup. Attach tubing to the 15 G Luer stub adapter. Close the side port of the stopcock with an unvented universal lock cap. Repeat for a total of two setups.
    3. Label one syringe as channel 1 intracranial pressure (CH1 ICP) and the other syringe as channel 2 intraocular pressure (CH2 IOP).
2. Set up outflow syringes (IOP and ICP reservoirs).
    1. Attach a 3-way stopcock to a 30 mL syringe. Attach a 15 G Luer stub adapter to the 3-way stopcock. Attach tubing to the 15 G Luer stub adapter.
    2. Close the side port of the stopcock with an unvented universal lock cap. Repeat for a total of two setups. Label one syringe as CH1 ICP and the other syringe as CH2 IOP.

4. Preparation of human whole eye globe

NOTE: If whole eyes are received, follow the procedure below to separate the anterior segment from the posterior segment of the eye. If the eyes are received bisected, start at step 4.4.

1. Place a whole eye into povidone-iodine solution for 2 min.
2. Rinse the eye in sterile phosphate buffered solution (PBS) to rinse off the povidone-iodine. Repeat 2 times.
3. Remove the adnexa from the whole eye globe using forceps and scissors. Bisect the eye at the equator to separate the anterior and posterior segments of the eye.
4. Remove the optic nerve sheath. Remove the vitreous humor from the posterior segment.
5. Trim additional sclera from posterior segment, if needed, to ensure a good fit on the round dome of the IOP (bottom) chamber. Using forceps, ensure that the retina is spread evenly over the posterior of the segment.
6. IOP (bottom) chamber setup
    1. Place the human posterior segment into the IOP (bottom) chamber of the TAS over the round dome with the optic nerve facing the top.
    2. Seal the posterior segment using the epoxy resin O-ring with four screws, ensuring a tight seal.
    3. Insert the tubing into the IN and OUT ports of the IOP (bottom) chamber. The IOP inflow syringe with tubing containing medium is inserted into the IN port and the empty IOP outflow syringe with tubing is inserted into the OUT port.

4. Use the push/pull method to slowly infuse the perfusion medium into the inflow port to fill the posterior eye cup while simultaneously slowly pulling the perfusion medium out through the outflow syringe to remove any air bubbles from the lines. Stop infusing medium once both the IN and OUT tubes are void of air bubbles.

5. Lock the stopcocks in the off position. Remove the 30 mL syringe from the IOP IN port filter assembly and refill with a total of 30 mL of medium. Replace the 30 mL syringe onto the filter assembly.

7. **ICP (top) chamber setup**

1. Place the ICP (top) chamber/lid over the back of the posterior segment. Make certain that the optic nerve is within the top chamber. Seal the top chamber with four screws.

2. Insert the tubing into the IN and OUT ports of the ICP (top) chamber. The ICP inflow syringe with tubing containing medium is inserted into the IN port and the empty ICP outflow syringe with tubing is inserted into the OUT port.

3. Gently and slowly infuse the medium into the IN port to fill the ICP chamber and remove air bubbles from the lines using the push/pull method. Stop infusing medium once the ICP chamber as well as both the IN and OUT tubing are void of air bubbles.

4. Lock the stopcocks in the off position. Remove the 30 mL syringe from the ICP in port filter assembly and refill with a total of 30 mL of medium. Replace the 30 mL syringe onto the filter assembly.

5. Data recording system setup

NOTE: The data recording system is comprised of an 8-channel power source, multichannel bridge amplifier, hydrostatic pressure transducers, and a computer with data acquisition software (see **Table of Materials**). The following describes how to set up and calibrate the system.

1. Connect the power cord into the back of the 8-channel power source and plug into a battery back-up device.

2. Connect the USB cable from the 8-channel power source into the back of the computer.

3. Connect the 8-channel power source to the multichannel bridge amplifier using the supplied I2C cord.

4. Connect the Bayonet Neill-Concelman (BNC) cables into the channel inputs in front of the 8-channel power source and the end of the cables into the corresponding channels in the back of the multichannel amplifier.

5. Connect the transducer cables to the front of the multichannel amplifier.

6. Install the data acquisition software on the computer.

    1. Run the data acquisition software setup installer from the supplied software CD.

    2. Follow the instructions on the computer screen.

    3. When the installation is complete, select **Finish**.

7. Turn on the 8-channel power source.

8. Turn on the computer and initiate the data acquisition software.

    1. Select **File** | **New.**

    2. Select **Setup** | **Channel Settings**. Select three channels (bottom left of screen). In the **Channel**

Title column rename the channels as follows: CH1 ICP; CH2 IOP; CH3 TLPG (IOP-ICP).

3. Select 2 mV for the **Range** on all channels. In the **Calculation** column select **No Calculation** for channels 1 and 2.

4. In the **Calculation** column select **Arithmetic** for channel 3. In the **Formula** section: Select **channels/ CH2**; Select **arithmetic "-"**; Select **channels/CH1**. In the **Output** section select **mmHg**. Select **OK**. Select **OK** again.

9. Set up and calibrate the hydrostatic pressure transducers.

NOTE: Hydrostatic pressure transducers must be calibrated prior to experiments using the following method.

1. Connect the hydrostatic pressure transducers to the transducer lines attached to the multichannel bridge amplifier.

2. Attach a 30 mL syringe filled with air to the side port of the CH1 (ICP) pressure transducer. Attach the sphygmomanometer to the bottom of the CH1 (ICP) pressure transducer.

3. On the chart, view the page of the data acquisition software, set the sampling speed by left clicking the arrow next to the sampling time and select **100**. Then right click in the **CH1** (ICP) area of the page.

4. Select **Bridge Amp**. Select **Mains Filter**. Select **Zero** and wait for the system to zero out, taking care to not move the pressure transducer.

5. Pinch the white tabs of the pressure transducer and push air through the transducer until 40 mmHg is obtained on the sphygmomanometer. Release the white tabs and remove the syringe and sphygmomanometer.

6. On the **Units Conversion** page, select '**minus (-)**' sign. Highlight the highest plateau to indicate 40 mmHg. Click the **Arrow** for point 1 and enter 40.

7. Highlight the lowest plateau to indicate 0 mmHg. Click the **Arrow** for point 2 and enter 0. Select mmHg for the units. Select **OK**.

8. Select **OK** (Bridge Amp page). Repeat steps 9.1–9.7 for CH2 (IOP) using 100 mmHg for the highest plateau and 0 for the lowest plateau.

10. Connect the TAS/posterior segment unit onto the data acquisition system.

1. Place the TAS/posterior segment unit into an incubator (37 °C, 5% CO_2). Attach the ICP tubing from the OUT port to the CH1 (ICP) pressure transducer.

2. Attach the IOP tubing from the OUT port to the CH2 (IOP) pressure transducer.

3. Attach the syringe setups (ICP and IOP) with medium from the IN ports to the ring stand.

4. On the **Chart view** page select **Start Sampling**. Set the sampling speed by left clicking the arrow next to the sampling time and select **Slow** and **1 min**.

5. Adjust the syringes on the ring stand up or down to regulate ICP and IOP pressures to protocol requirements.

6. Perform systemic replenishment of medium in the system every 48–72 h through the push and pull method.

6. Data retrieval and analysis

1. Open the data file in the data acquisition software.
2. In the **Data Pad** section, click on the **Multiple Add to Data Pad** icon. A new window will appear.
    1. In the **Find Using** section select **Time** from the drop-down menu.
    2. In the **Select** section select **1 hr** every **1 hr** from the drop-down menus.
    3. In the **Step Through** section select **Whole File** then click **Add**.
3. In the **Data Pad** section click on the **Data Pad View** icon. Highlight all the data and copy/paste into a spreadsheet.
4. Calculate the mean and standard deviations for IOP, ICP, and TLPG for every 24 h. Collate the data using the pivot table option in a spreadsheet program and graph.

7. Immunohistochemistry and hematoxylin and eosin staining of posterior segments

1. Remove the posterior eye segments following various timepoints from the TAS model and fix in formalin prior to paraffinizing.
2. Section the eyes to produce sagittal tissue planes.
3. Deparaffinize the paraffin-embedded segments with a 100% xylene, 95% ethanol, 50% ethanol solution.
4. Wash the slides with PBS for 10 min and block with a blocking buffer at room temperature for 1 h.
5. Label sections with primary antibodies: anti-collagen IV (Extracellular Matrix (ECM) marker, NB120-6586, 1:100) and anti-laminin (ECM marker, NB300-144, 1:100, anti-RBPMS (RGC marker), GTX118619, 1:50).
6. Detect the primary antibodies using Alexa Fluor secondary antibodies (Alexa Fluor 488 goat anti-rabbit, A11008, 1:500).
7. Counterstain the cell nuclei using DAPI anti-fade solution.
8. Capture images of the stained sections and phase images with 4x and 10x objective lenses using a fluorescence microscope (see **Table of Materials**).
9. For the hematoxylin and eosin (H&E) staining, process the sections in an automated staining system (see **Table of Materials**) for deparaffinization using a 100%, xylene 95% ethanol, 50% ethanol solution and stain with H&E.
10. Capture images with the 4x and 10x objective lenses using a microscope with a bright field light source.

Representative Results

Design and creation of the translaminar autonomous system

Translaminar pressure differential is a potential key mechanism in the pathogenesis of various diseases, including glaucoma. Uses for the model described include, but are not limited to, the study of glaucoma (elevated IOP, perhaps decreased ICP), traumatic brain injury (elevated ICP), and long-term exposure to microgravity-associated visual impairment (elevated ICP, elevated IOP). To help discover molecular pathogenesis targeting translaminar pressure in the human eye, we designed, created, and validated the TAS model. Our novel ex vivo human model gives a unique preclinical system to independently study ICP and IOP-associated pathogenic changes. To address human preclinical applications, our model provides an ex vivo paradigm of studying pathogenesis due to translaminar pressure changes. The sealed model design is depicted with

solid front and transparent views (**Figure 1A**, **1B**) with a detailed diagrammatic view of the model to depict all the inflow and outflow ports (**Figure 1C**). The color transparent view with a human posterior segment in an actual 3D printed model is shown (**Figure 1D**, **1E**).

Translaminar Autonomous System: A novel ex vivo human translaminar pressure model

We generated the TAS model with two autonomous chambers (i.e., IOP and ICP chambers). In the bottom base of the model, the human posterior cup was placed over the top of the round dome with the optic nerve facing the top. Once the posterior cup was placed and sealed in the IOP chamber, we placed the ICP chamber on top of the nerve. We maintained the independence of both chambers and a perfect seal using O-rings that fit each chamber precisely (**Figure 2A**). The bottom chamber or the IOP chamber filled and regulated pressure in the cup, while the top chamber fit around the optic nerve and regulated the ICP around the nerve through hydrostatic pressure reservoirs. Using the model, we independently regulated IOP and ICP using hydrostatic pressure. The difference between both chambers was identified as a change in translaminar pressure gradient (**Figure 2B**). The model depicted with all final fittings in place including the inflow and outflow reservoir syringes connected is shown in **Figure 2C**.

Successful culture and pressure maintenance in the translaminar autonomous system

To ensure that both chambers worked independently in the system, we regulated several pressure differentials by keeping the IOP chamber and ICP at different average pressure differentials (normal TLPG: IOP: ICP, 15:5 mmHg; elevated TLPG >10 mmHg; elevated TLPG >20 mmHg). We initially tested the maintenance of average normal pressure differentials in both chambers (normal IOP/ICP) through various different parameters of IOP and ICP conditions: 1) normal IOP: decreased ICP (**Figure 3A**); 2) elevated IOP: decreased ICP (**Figure 3B**); and 3) elevated IOP: elevated ICP (**Figure 3C**). The average normal IOP ranges from 10–21 mmHg (episcleral venous pressure factored in) and normal ICP from 5–15 mmHg. In lieu of the limitation of not having vascular pressure, we still maintained the pressure to these rates, as the idea was to exert the maximal pressure at the ONH. We independently regulated various pressure levels in both chambers (ICP, 5–10 mmHg; IOP, 20–40 mmHg). To ensure pressure maintenance between both chambers, we kept IOP under normal conditions (15 mmHg) and decreased ICP (4 mmHg) to sustain a TLPG (IOP-ICP) between the LC of 11 mmHg (**Figure 3A**). We then elevated IOP (43 mmHg) and decreased ICP (3 mmHg) (**Figure 3B**) and finally elevated pressures in both (IOP, 64 mmHg; ICP, 9 mmHg) to generate the largest level of TLPG at 55 mmHg (**Figure 3C**). To ensure the viability of the tissue (**Figure 4**), the medium in the tissues was exchanged every 48 h by attaching an empty syringe to the outflow stopcock and slowly pushing approximately 5 mL of perfusion medium through the inflow port using the push/pull method. Minimal pressure increases occurred at the time of medium exchange (**Figure 4G**) and did not affect the morphology of the ONH as shown in the 14- and 30 day immunohistochemistry data (**Figure 4A**–**F**). To confirm that we could culture posterior segments for extended timeframes with effective viability within the TAS model, we analyzed cross sections of the ONH after maintenance of normal IOP and ICP for 14 and 30 days. We were able to successfully culture these segments in the model for 14 days (**Figure 4A**, **4B**) with healthy ONH cells and extracellular matrix expression of collagen IV (COLIV) at the optic nerve head (**Figure 4C**). Similar viability and maintenance of the posterior segment was also observed for 30 days (**Figure 4D**,

4E) with expression of COLIV and DAPI (**Figure 4F**). The graphical representation of TLPG (IOP-ICP) values (**Figure 4G**) depicts a constant maintenance of IOP values over time at 15.6 ± 4.6 mmHg and ICP mean at 11.0 ± 4.6 mmHg for 30 days with a TLPG of 4.6 ± 1.3 mmHg (**Table 1**).

Morphological changes to the ONH post elevated translaminar pressure gradient

A common clinical feature of the age-related neurodegenerative disease glaucoma is ONH cupping. Prelaminar cupping is distinguished by progressive loss of prelaminar neural tissues, which increases both the depth and width of the cup and thus increases the cup-to-disk ratio. Laminar cupping is connective tissue-based, with the LC moving posteriorly progressively and excavating. Glaucomatous cupping is a combination of these two components, reflecting both damage and remodeling of laminar connective tissues. Elevation in IOP leads to LC thickening due to an increase in collagen fibril mass[53]. Utilizing the TAS model, we created an elevated TLPG by increasing IOP or decreasing ICP over various timepoints. We maintained a range of elevated TLPG for 7 days with average IOP values over time at 22.8 ± 18.6 mmHg and ICP mean at 6.9 ± 7.6 mmHg with a TLPG of 15.9 ± 11.8 mmHg (**Table 2**). The highest TLPGs were documented at 36 mmHg. Human posterior segments were then analyzed morphologically for progressive thickening of laminar beams and cupping at the ONH in H&E stained sections as time progressed between control, 1 day, 3 days, and 7 days under elevated TLPG (**Figure 5A**–**D**). Cupping and thickening were observed at 7 days of elevated TLPG (**Figure 5D**). Further, COLIV expression over time between control, 1 day, 3 days, and 7 days showed thickened beams and increased expression by 7 days (**Figure 5E**–**H**). Phase images comparing control tissue not cultured in the TAS model (**Figure 5I**) and 7 days (**Figure 5J**) of elevated TLPG within the TAS model show healthy RGCs within the GCL (**Figure 5I**) with no cupping (**Figure 5I**) for the control, while under conditions of elevated TLPG the images show extensive cupping with no remaining RGCs (RBPMS-RGC marker) in the RNFL (**Figure 5J**) and increased remodeling of ECM as shown by elevated COLIV within the ONH (**Figure 5J**).

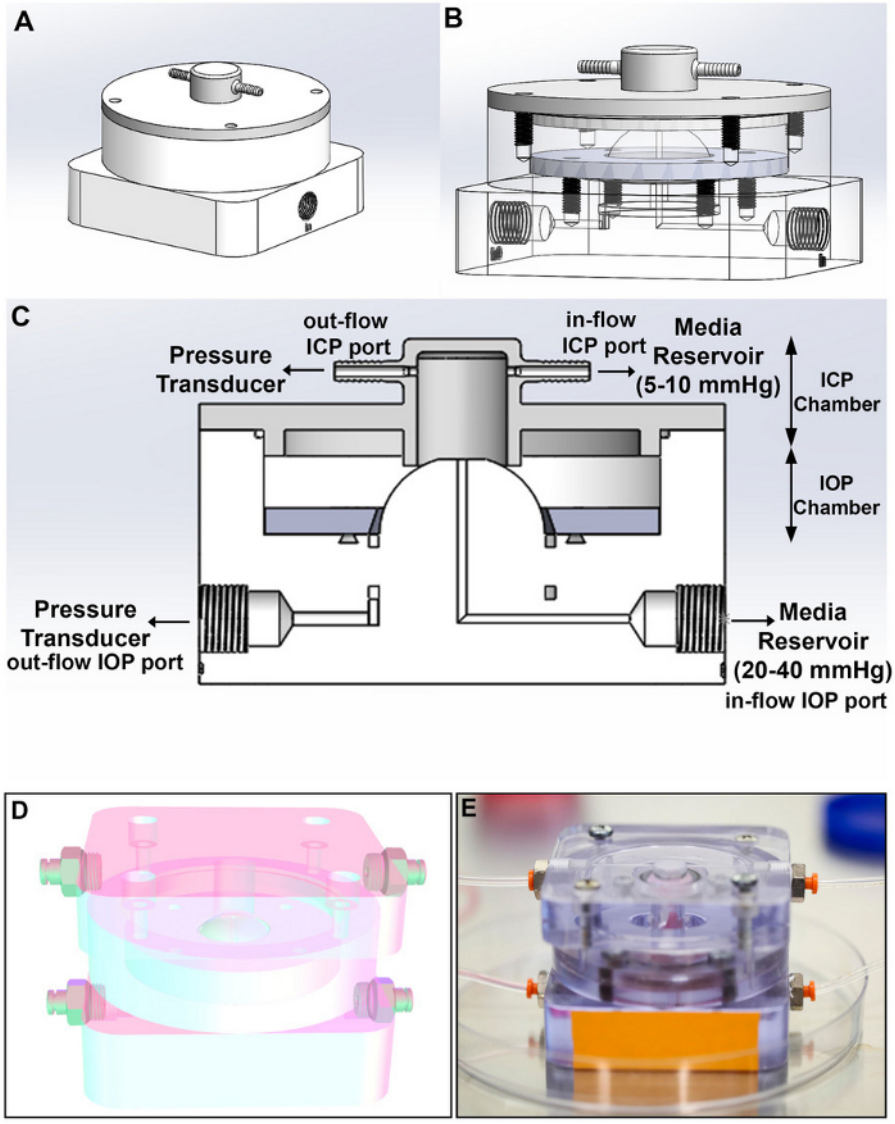

Figure 1: Translaminar autonomous system. Model depiction. (**A**) Solid front view. (**B**) Transparent view. (**C**) Diagrammatic view. (**D**) Color transparent view. (**E**) Actual 3D printed model. Please click here to view a larger version of this figure.

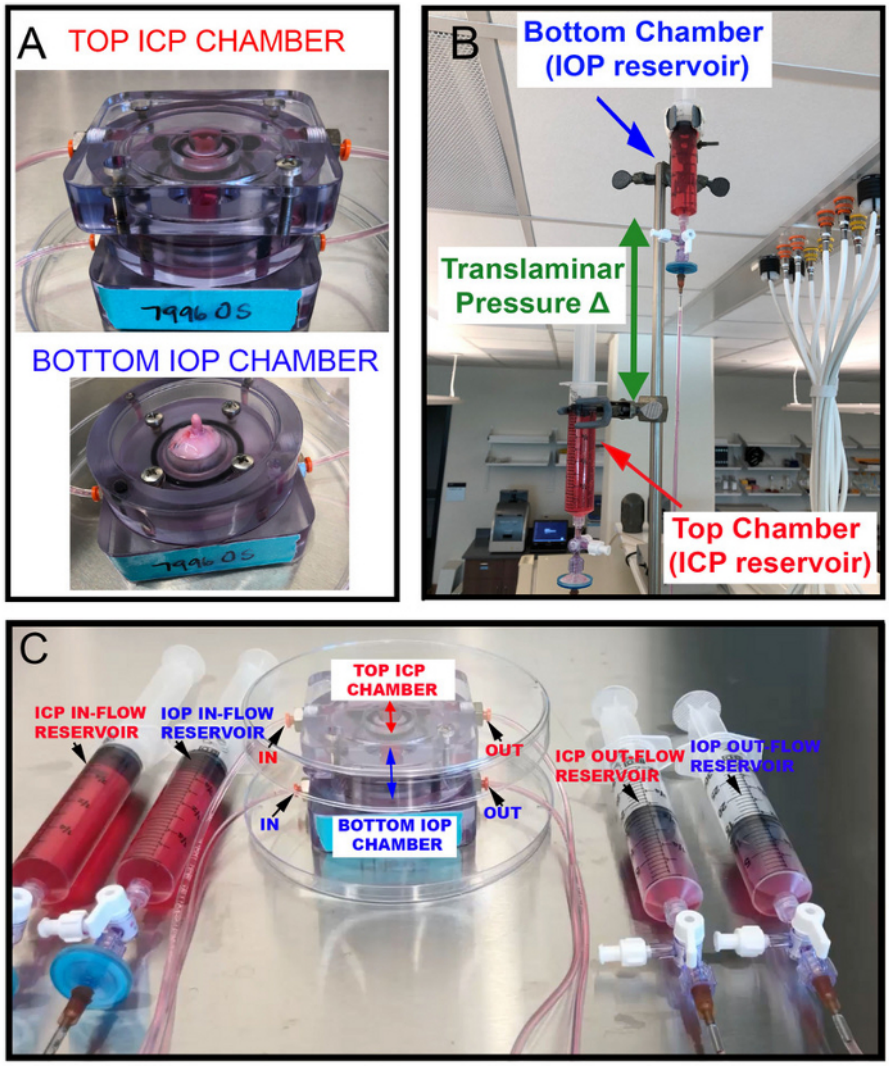

Figure 2: Mechanics of the translaminar autonomous system. (**A**) The TAS model with ICP and IOP chambers for regulating translaminar pressure differentials. (**B**) Depiction of the TAS model with autonomous regulation of hydrostatic pressure in both chambers through elevation of reservoirs. (**C**) Image of the TAS model with all the fittings in place and representation of the inflow and outflow reservoir syringes. Please click here to view a larger version of this figure.

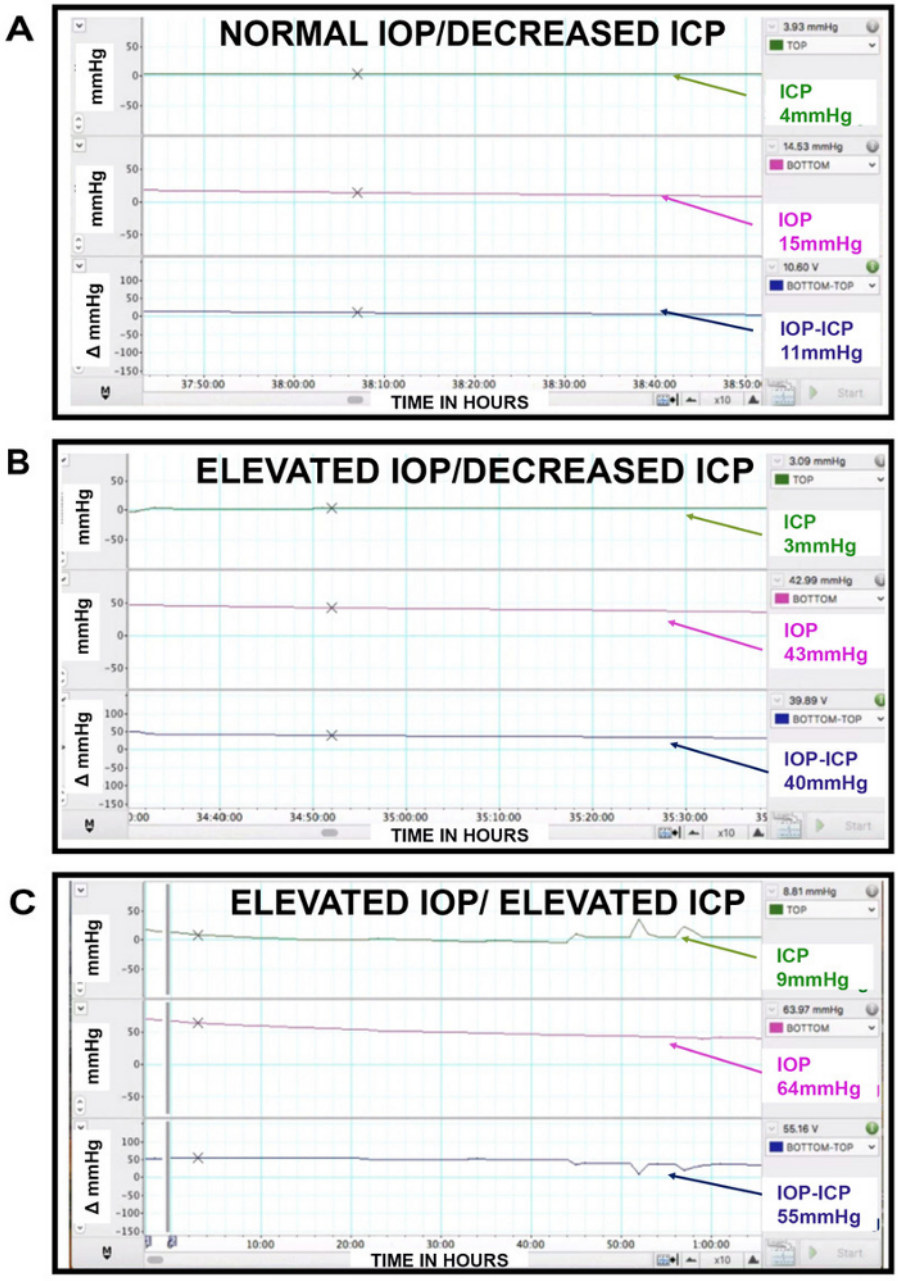

Figure 3: Independent pressure maintenance within the translaminar autonomous system. Graphical representation of pressures being independently modulated, and stable pressures being maintained in the top (ICP) and bottom (IOP) chambers with (**A**) normal IOP/decreased ICP (**B**) elevated IOP/decreased ICP, and (**C**) elevated IOP/elevated ICP. Please click here to view a larger version of this figure.

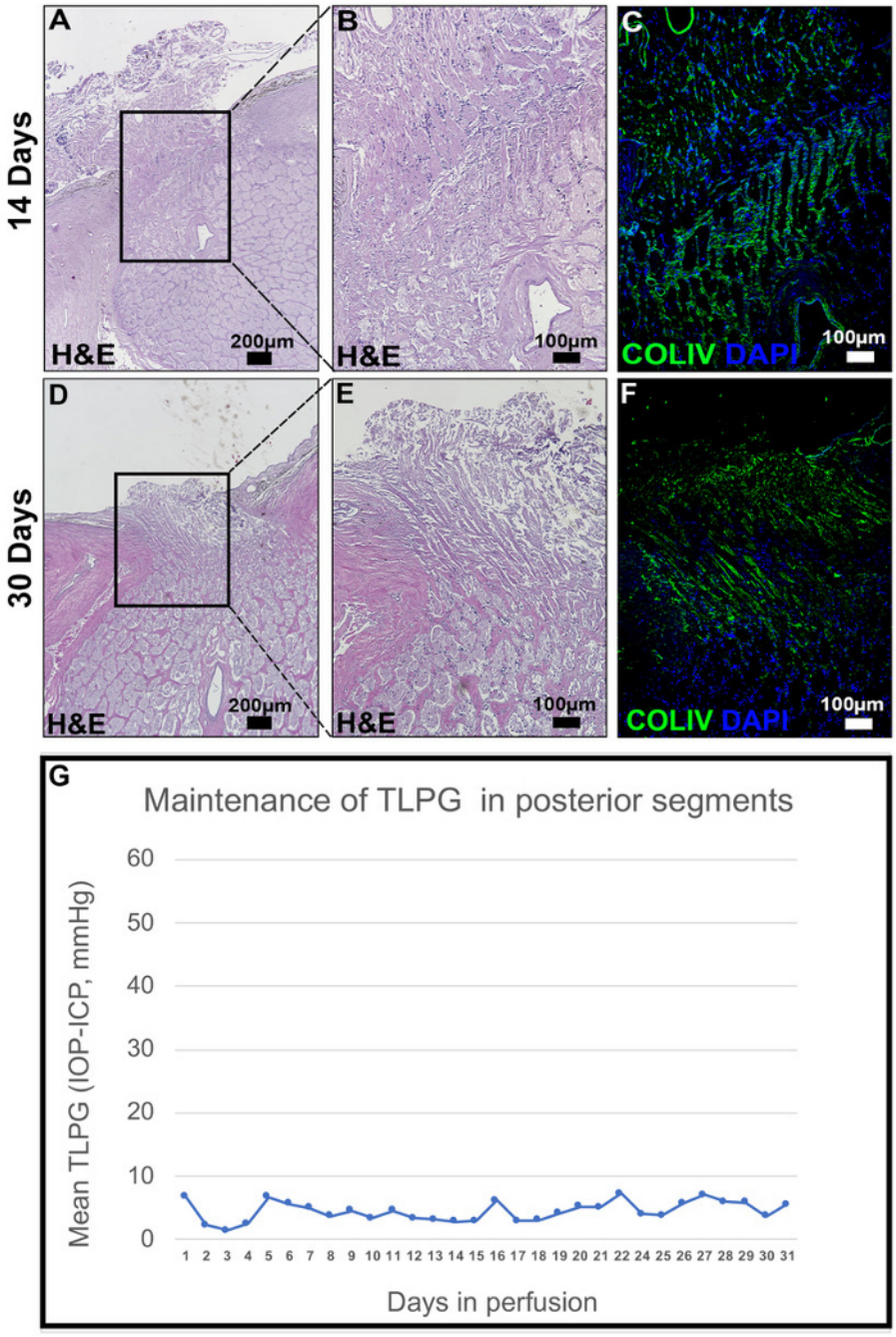

Figure 4: Maintenance and viability of posterior segments within the translaminar autonomous system. Human posterior segments were cultured using the TAS model for 14 and 30 days under normal conditions of IOP and ICP. H&E stained cross sections of human ONH at 14 days in (**A**) low magnification (40x) and (**B**) high magnification (100x). (**C**) COLIV immunostaining with DAPI expression (100x). Similar depictions of H&E staining at 30 days in (**D**) 40x and (**E**) 100x micrographs and (**F**) COLIV immunostaining with DAPI expression (100x). **G**) Graphical presentation of Δ in mmHg of IOP-ICP (TLPG) for human posterior segments maintained for 30 days in culture. COLIV = green; DAPI = blue; (**A**, inset **B**); (**D**, inset **E**); H&E = hematoxylin and eosin stain. Please click here to view a larger version of this figure.

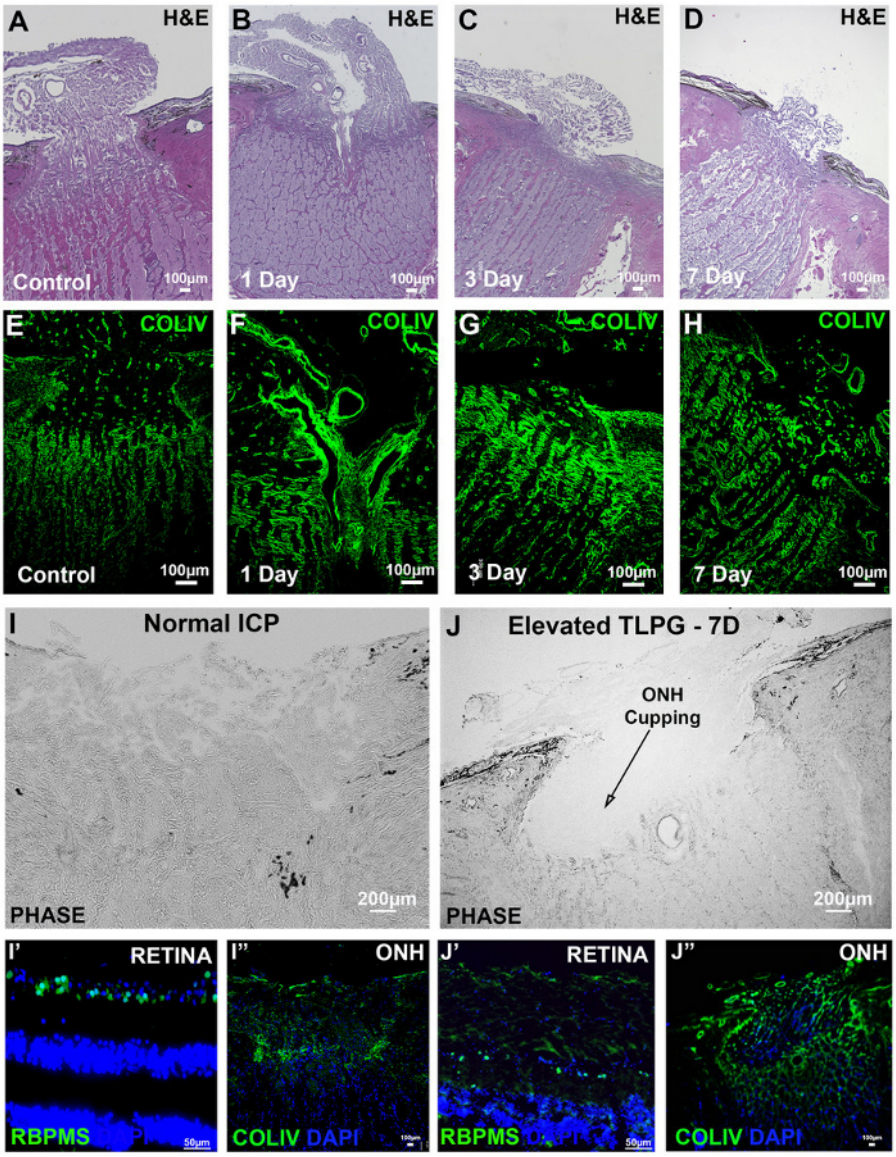

Figure 5: Morphological restructuring of the optic nerve head after elevated translaminar pressure gradient in the Translaminar Autonomous System. Human posterior segments were cultured using the TAS model for various time points under elevated TLPG conditions. Cross sections of human ONH depicting H&E staining of (**A**) control (**B**) 1 day in TAS (**C**) 3 days in TAS, and (**D**) 7 days of culture. Expression of COLIV with DAPI in the ONH of (**E**) control (**F**) 1 day in TAS (**G**) 3 days in TAS, and (**H**) 7 days in culture. Phase contrast ONH cross section images of (**I**) control ONH depicting (**I'**) retina staining of RBPMS and (**I''**) ONH staining with COLIV and DAPI. Phase contrast of (**J**) 7 days of elevated TLPG in TAS with insets depicting (**J'**) retina staining of RBPMS and (**J''**) ONH staining with COLIV and DAPI. COLIV, RBPMS = green; DAPI = blue; (**A**–**D**) 40x magnification; (**E**–**H**) 100x Magnification; (**I** and **J**) 200x magnification; (**J'**) 400x magnification; (**J''**) 100x magnification; (**J**, inset **J'** and **J''**); H&E = hematoxylin and eosin stain; TAS = Translaminar Autonomous System. Please click here to view a larger version of this figure.

Days	Mean IOP of 24 h	Mean ICP of 24 h	Mean TLPG (IOP-ICP)
1	17.7	12.1	5.7
2	20.0	15.0	5.0
3	13.4	9.6	3.7
4	15.1	10.5	4.5
5	11.6	8.3	3.3
6	14.0	9.5	4.5
7	17.2	13.8	3.4
8	19.3	16.1	3.2
9	17.7	15.0	2.8
10	10.9	8.0	2.9
11	16.3	10.2	6.1
12	14.7	11.8	2.9
13	7.5	4.5	3.0
14	5.5	1.4	4.1
15	13.5	8.3	5.2
16	15.4	10.3	5.1
17	11.7	4.5	7.3
18	13.3	9.3	4.0
19	23.5	19.7	3.8
20	20.3	14.5	5.7
21	12.8	5.8	7.0
22	25.8	19.9	5.9
23	19.3	13.5	5.8
24	18.8	15.1	3.7
25	14.4	8.9	5.5
AVG	**15.6**	**11.0**	**4.6**

STD	**4.6**	**4.6**	**1.3**

Table 1: Maintenance of normal TLPG maintained for 30 days. Tabular values depicting IOP, ICP, and TLPG values every 24 h with average and standard deviation over the complete time course.

Days	Mean IOP of 24 h	Mean ICP of 24 h	Mean TLPG of 24 h
1	4.1	-1.0	5.1
2	6.3	1.1	5.3
3	13.4	4.0	9.4
4	19.0	1.1	17.9
5	55.6	19.5	36.2
6	39.5	12.8	26.7
7	21.5	10.8	10.6
AVG	**22.8**	**6.9**	**15.9**
STD	**18.6**	**7.6**	**11.8**

Table 2: Maintenance of a range of elevated TLPG maintained for 7 days. Tabular values depicting IOP, ICP, and TLPG values every 24 h with average and standard deviation over the complete time course.

Supplemental Figure 1: Ex vivo human retinal explant culture. Phase contrast, RGC positive stained (RBPMS-green), and cellular (DAPI-blue) stained images of retinal explants in culture for (**A**–**C**) 7 days and (**D**–**F**) 14 days (200x magnification). Please click here to download this figure.

Supplemental Figure 2: Human adult RGC cultures. RGC marker (RBPMS-green) and DAPI (blue) stained RGCs 7 days in culture (**A**) 200x (**B**) 400x magnification. (**C**) RGCs stained for NEFL (green) and DAPI (blue) at 400x magnification. Please click here to download this figure.

Discussion

Human postmortem tissues are an especially valuable resource for studying human neurodegenerative diseases because identification of potential drugs developed in animal models need to be translatable to humans[47]. The effects of human IOP elevation are well-established, but minimal research has been performed on abnormal ONH translaminar pressure changes. Even though multiple animal models and finite modeling of human ONH exist, there is no ex vivo human model to study translaminar pressure changes[41,54,55,56,57]. A current unmet need exists for a new preclinical human model that can target disease etiology ex vivo using IOP and ICP and can identify various

pathogenic paradigms related to glaucoma pathogenesis. Understanding pressure-related pathological changes at the ONH will be crucial to preventing RGC death. The combined use of IOP, ICP, and TLPG within the TAS model is a unique approach to study pressure-dependent degeneration in a preclinical manner utilizing human posterior segment tissue. In the TAS model, we can culture posterior segments of human eye cups to study changes of translaminar pressure through autonomous regulation of the IOP and ICP chambers. It provides a foundation for developing a new range of therapeutics that focus on translaminar pressure as a mechanism of degeneration.

Setting up the TAS model requires attention to detail in many aspects: the correct dissection of the human posterior segments, ensuring that the retina is in intact and spread over the posterior cup, proper placement of the segment over the dome of the IOP chamber, accurately situating the ICP chamber over the ON, effective sealing of both chambers, and maintenance of hydrostatic pressures independently by regulating height of IOP and ICP reservoirs. Dissection needs to be performed in eyes that are no more than 24–36 h postmortem, because the retina progressively deteriorates if effective culture medium is not replenished. Systemic replenishment of medium was performed in our system every 48–72 h. Another crucial aspect of the system is the length of the ON. It is critical to ensure that at least 0.5–1 cm of ON is left on the cadaveric eye. Donor eyes should not be used if they have short ONs, the ON is damaged, the globe is compromised and deflated, or the ON sheath is detached. Further, when placing the posterior segment over the dome, the O-ring must be tightly fit in place and the top ICP chamber correctly sealed with screws. The pushpin fittings where the tubing attaches on each side of the top and bottom base of the model also need to be tested to ensure that the tubing fits

and locks in place. If the tubing is not properly in place, air bubbles will be observed within the tubing and compromise the pressure measurements within each chamber.

Maintenance and viability of the postmortem posterior segments in our TAS model was a critical concern for this protocol. Human postmortem tissue has previously been extensively studied[48,49], with a recent RNA analysis study of 1,068 postmortem donor tissues confirming that postmortem human brain tissue collected over decades can serve as high-quality material for study of human disorders[47]. In addition, previously successful expression profiling of ocular human donor eye tissues postmortem has been performed[58]. Gene expression PLIER values for apoptosis genes were minimal or nonexistent in this dataset for retinal tissue 6 h postmortem[58]. Furthermore, it has been shown that hypothermic storage of eye tissue can be performed effectively[59]. It has been shown that ganglion cell activity is maintained for 50 h when minipig eyes are stored at ischemic and hypothermic conditions[41,60]. Therefore, we used the 6 h time point as our inclusion criteria for donor eyecup collection. The speed of postmortem deterioration of posterior segments and retinal detachment is lacking in the literature, but our enucleation within 6 h, delivery over ice, and culture setup of maximal 36 h is well within the range of tissue viability as depicted in **Supplemental Figure 1** and **Supplemental Figure 2**. Using the TAS model, we successfully achieved healthy maintenance of tissue for 30 days.

Another limitation of the TAS model is our current inability to model the cyclic circadian rhythms of ICP and IOP that are observed under normal physiological conditions. This can be addressed in the future by using a pump that can regulate rhythmic IOP and ICP infusion. Further, another caveat to the model is the lack of blood circulation within the cadaveric eye.

Thus, the effects of blood pressure cannot be studied, but this also allows us to specifically delineate the pathogenic effects of only TLPG changes, including IOP and ICP.

A future scope of the model would incorporate automation of the reservoir systems for hydrostatic changes and perfusion of medium through an infusion pump with an exit empty syringe on the transducer instead of the multiple rounds of medium change that were implemented in this protocol. The fluid from the IOP and ICP reservoir could also be collected and analyzed. Medium can be collected for biomarker expression to target future therapies. We can also identify pathways or molecules that can be treated with drugs or gene therapy and test these therapies in various animal models of ICP before translation to human clinical trials.

In conclusion, our model not only provides a human basis of testing, but it can also be utilized to validate therapies that can target translaminar pressure changes in the eye. It opens an avenue to perform precision medicine through transplantation of patient stem cells on human donor eyecups and pressurize them in the TAS model. This allows us to test therapies ex vivo with the capacity to be translatable to the clinic and relatable to living individuals. With our model we can now assess the changes occurring in translaminar pressure and how it plays a crucial role in the pathogenesis associated with various traumatic and neurodegenerative diseases. This will lead to a better understanding of pathogenic molecular mechanisms in the ONH that are associated with IOP and ICP.

Disclosures

The authors of the manuscript have no potential conflicts of interest to disclose.

Acknowledgments

Funding for this project was through discretionary funds of Dr. Colleen M. McDowell. This work was supported in part by an unrestricted grant from Research to Prevent Blindness, Inc. to the UW Madison Department of Ophthalmology and Visual Sciences. We thank Drs. Abbot F. Clark and Weiming Mao for their technical assistance with the perfusion organ culture model. We thank the Lions Eye Institute for Transplant and Research (Tampa, FL) for providing the human donor eyes.

References

1. Pascolini, D., Mariotti, S. P. Global estimates of visual impairment: 2010. *The British Journal of Ophthalmology.* **96** (5), 614–618 (2012).
2. Bastawrous, A. et al. Posterior segment eye disease in sub-Saharan Africa: review of recent population-based studies. *Tropical Medicine & International Health.* **19** (5), 600–609 (2014).
3. Morgan, J. E. Circulation and axonal transport in the optic nerve. *Eye.* **18** (11), 1089–1095 (2004).
4. Burgoyne, C. F. A biomechanical paradigm for axonal insult within the optic nerve head in aging and glaucoma. *Experimental Eye Research.* **93** (2), 120–132 (2011).
5. Quigley, H. A., Addicks, E. M. Chronic experimental glaucoma in primates. II. Effect of extended intraocular pressure elevation on optic nerve head and axonal transport. *Investigative Ophthalmology, Visual Science.* **19** (2), 137–152 (1980).
6. Quigley, H. A., Addicks, E. M., Green, W. R., Maumenee, A. E. Optic nerve damage in human glaucoma. II. The site of injury and susceptibility to damage. *Archives of Ophthalmology.* **99** (4), 635–649 (1981).

7. Howell, G. R. et al. Axons of retinal ganglion cells are insulted in the optic nerve early in DBA/2J glaucoma. *The Journal of Cell Biology.* **179** (7), 1523–1537 (2007).
8. Johnson, E. C., Jia, L., Cepurna, W. O., Doser, T. A., Morrison, J. C. Global changes in optic nerve head gene expression after exposure to elevated intraocular pressure in a rat glaucoma model. *Investigative Ophthalmology, Visual Science.* **48** (7), 3161–3177 (2007).
9. Howell, G. R. et al. Molecular clustering identifies complement and endothelin induction as early events in a mouse model of glaucoma. *Journal of Clinical Investigation.* **121** (4), 1429–1444 (2011).
10. Qu, J., Jakobs, T. C. The Time Course of Gene Expression during Reactive Gliosis in the Optic Nerve. *PloS one.* **8** (6), e67094 (2013).
11. Berdahl, J. P., Fautsch, M. P., Stinnett, S. S., Allingham, R. R. Intracranial pressure in primary open angle glaucoma, normal tension glaucoma, and ocular hypertension: a case-control study. *Investigative Ophthalmology, Visual Science.* **49** (12), 5412–5418 (2008).
12. Berdahl, J. P., Allingham, R. R. Intracranial pressure and glaucoma. *Current Opinion in Ophthalmology.* **21** (2), 106–111 (2010).
13. Morgan, W. H. et al. The correlation between cerebrospinal fluid pressure and retrolaminar tissue pressure. *Investigative Ophthalmology, Visual Science.* **39** (8), 1419–1428 (1998).
14. Leske, M. C., Connell, A. M., Wu, S. Y., Hyman, L. G., Schachat, A. P. Risk factors for open-angle glaucoma.

The Barbados Eye Study. *Archives of Ophthalmology.* **113** (7), 918–924 (1995).

15. Quigley, H. A., Green, W. R. The histology of human glaucoma cupping and optic nerve damage: clinicopathologic correlation in 21 eyes. *Ophthalmology.* **86** (10), 1803–1830 (1979).
16. Burgoyne, C. F., Downs, J. C., Bellezza, A. J., Hart, R. T. Three-dimensional reconstruction of normal and early glaucoma monkey optic nerve head connective tissues. *Investigative Ophthalmology, Visual Science.* **45** (12), 4388–4399 (2004).
17. Diekmann, H., Fischer, D. Glaucoma and optic nerve repair. *Cell and Tissue Research.* **353** (2), 327–337 (2013).
18. Nickells, R. W., Howell, G. R., Soto, I., John, S. W. Under pressure: cellular and molecular responses during glaucoma, a common neurodegeneration with axonopathy. *Annual Review of Neuroscience.* **35**, 153–179 (2012).
19. Burgoyne, C. F., Downs, J. C. Premise and prediction-how optic nerve head biomechanics underlies the susceptibility and clinical behavior of the aged optic nerve head. *Journal of Glaucoma.* **17** (4), 318–328 (2008).
20. Sigal, I. A., Ethier, C. R. Biomechanics of the optic nerve head. *Experimental Eye Research.* **88** (4), 799–807 (2009).
21. Sigal, I. A., Flanagan, J. G., Tertinegg, I., Ethier, C. R. Modeling individual-specific human optic nerve head biomechanics. Part I: IOP-induced deformations and influence of geometry. *Biomechanics and Modeling in Mechanobiology.* **8** (2), 85–98 (2009).

22. Morgan, J. E., Jeffery, G., Foss, A. J. Axon deviation in the human lamina cribrosa. *The British Journal of Ophthalmology.* **82** (6), 680–683 (1998).

23. Danias, J. et al. Quantitative analysis of retinal ganglion cell (RGC) loss in aging DBA/2NNia glaucomatous mice: comparison with RGC loss in aging C57/BL6 mice. *Investigative Ophthalmology, Visual Science.* **44** (12), 5151–5162 (2003).

24. Berdahl, J. P., Allingham, R. R., Johnson, D. H. Cerebrospinal fluid pressure is decreased in primary open-angle glaucoma. *Ophthalmology.* **115** (5), 763–768 (2008).

25. Fleischman, D., Allingham, R. R. The role of cerebrospinal fluid pressure in glaucoma and other ophthalmic diseases: A review. *Saudi Journal of Ophthalmology.* **27** (2), 97–106 (2013).

26. Morgan, W. H. et al. Optic disc movement with variations in intraocular and cerebrospinal fluid pressure. *Investigative Ophthalmology, Visual Science.* **43** (10), 3236–3242 (2002).

27. Feola, A. J. et al. Deformation of the Lamina Cribrosa and Optic Nerve Due to Changes in Cerebrospinal Fluid Pressure. *Investigative Ophthalmology & Visual Science.* **58** (4), 2070–2078 (2017).

28. Koeberle, P. D., Bahr, M. Growth and guidance cues for regenerating axons: where have they gone? *Journal of Neurobiology.* **59** (1), 162–180 (2004).

29. Kermer, P., Klocker, N., Bahr, M. Neuronal death after brain injury. Models, mechanisms, and therapeutic strategies in vivo. *Cell and Tissue Research.* **298** (3), 383–395 (1999).

30. Koeberle, P. D., Gauldie, J., Ball, A. K. Effects of adenoviral-mediated gene transfer of interleukin-10, interleukin-4, and transforming growth factor-beta on the survival of axotomized retinal ganglion cells. *Neuroscience.* **125** (4), 903–920 (2004).

31. Kipnis, J. et al. Neuronal survival after CNS insult is determined by a genetically encoded autoimmune response. *The Journal of Neuroscience : The Official Journal of the Society for Neuroscience.* **21** (13), 4564–4571 (2001).

32. Isenmann, S., Wahl, C., Krajewski, S., Reed, J. C., Bahr, M. Up-regulation of Bax protein in degenerating retinal ganglion cells precedes apoptotic cell death after optic nerve lesion in the rat. *The European Journal of Neuroscience.* **9** (8), 1763–1772 (1997).

33. Kermer, P. et al. Caspase-9: involvement in secondary death of axotomized rat retinal ganglion cells in vivo. *Brain research. Molecular Brain Research.* **85** (1-2), 144–150 (2000).

34. Kermer, P., Klocker, N., Labes, M., Bahr, M. Inhibition of CPP32-like proteases rescues axotomized retinal ganglion cells from secondary cell death in vivo. *The Journal of Neuroscience : The Official Journal of the Society for Neuroscience.* **18** (12), 4656–4662 (1998).

35. Kikuchi, M., Tenneti, L., Lipton, S. A. Role of p38 mitogen-activated protein kinase in axotomy-induced apoptosis of rat retinal ganglion cells. *The Journal of Neuroscience : The Official Journal of the Society for Neuroscience.* **20** (13), 5037–5044 (2000).

36. Barron, K. D., Dentinger, M. P., Krohel, G., Easton, S. K., Mankes, R. Qualitative and quantitative ultrastructural observations on retinal ganglion cell layer of rat after

intraorbital optic nerve crush. *Journal of Neurocytology.* **15** (3), 345–362 (1986).

37. Misantone, L. J., Gershenbaum, M., Murray, M. Viability of retinal ganglion cells after optic nerve crush in adult rats. *Journal of Neurocytology.* **13** (3), 449–465 (1984).
38. Bahr, M. Live or let die - retinal ganglion cell death and survival during development and in the lesioned adult CNS. *Trends in Neurosciences.* **23** (10), 483–490 (2000).
39. Klocker, N., Zerfowski, M., Gellrich, N. C., Bahr, M. Morphological and functional analysis of an incomplete CNS fiber tract lesion: graded crush of the rat optic nerve. *Journal of Neuroscience Methods.* **110** (1–2), 147–153 (2001).
40. Del Amo, E. M. et al. Pharmacokinetic aspects of retinal drug delivery. *Progress in Retinal and Eye Research.* **57**, 134–185 (2017).
41. Rousou, C. et al. A technical protocol for an experimental ex vivo model using arterially perfused porcine eyes. *Experimental Eye Research.* **181**, 171–177 (2019).
42. Vézina, M. *Assessing Ocular Toxicology in Laboratory Animals.* pp. 1–21 Humana Press, (2012).
43. de Boo, J., Hendriksen, C. Reduction strategies in animal research: a review of scientific approaches at the intra-experimental, supra-experimental and extra-experimental levels. *Alternatives to Laboratory Animals.* **33** (4), 369–377 (2005).
44. Kirk, R. G. W. Recovering The Principles of Humane Experimental Technique: The 3Rs and the Human Essence of Animal Research. *Science, Technology, & Human Values.* **43** (4), 622–648 (2018).
45. Burden, N., Chapman, K., Sewell, F., Robinson, V. Pioneering better science through the 3Rs: an

introduction to the national centre for the replacement, refinement, and reduction of animals in research (NC3Rs). *Journal of the American Association for Laboratory Animal Science.* **54** (2), 198–208 (2015).

46. Singh, J. The national centre for the replacement, refinement, and reduction of animals in research. *Journal of Pharmacology and Pharmacotherapeutics.* **3** (1), 87–89 (2012).

47. White, K. et al. Effect of Postmortem Interval and Years in Storage on RNA Quality of Tissue at a Repository of the NIH NeuroBioBank. *Biopreservation and Biobanking.* **16** (2), 148–157 (2018).

48. Ervin, J. F. et al. Postmortem delay has minimal effect on brain RNA integrity. *Journal of Neuropathology & Experimental Neurology.* **66** (12), 1093–1099 (2007).

49. Heinrich, M., Matt, K., Lutz-Bonengel, S., Schmidt, U. Successful RNA extraction from various human postmortem tissues. *International Journal of Legal Medicine.* **121** (2), 136–142 (2007).

50. Johnson, D. H., Tschumper, R. C. Human trabecular meshwork organ culture. A new method. *Investigative Ophthalmology, Visual Science.* **28** (6), 945–953 (1987).

51. Gottanka, J., Chan, D., Eichhorn, M., Lutjen-Drecoll, E., Ethier, C. R. Effects of TGF-beta2 in perfused human eyes. *Investigative Ophthalmology, Visual Science.* **45** (1), 153–158 (2004).

52. Pang, I. H., McCartney, M. D., Steely, H. T., Clark, A. F. Human ocular perfusion organ culture: a versatile ex vivo model for glaucoma research. *Journal of Glaucoma.* **9** (6), 468–479 (2000).

53. Aryee, M. J., Gutierrez-Pabello, J. A., Kramnik, I., Maiti, T., Quackenbush, J. An improved empirical

bayes approach to estimating differential gene expression in microarray time-course data: BETR (Bayesian Estimation of Temporal Regulation). *BMC Bioinformatics.* **10**, 409 (2009).

54. Feola, A. J. et al. Finite Element Modeling of Factors Influencing Optic Nerve Head Deformation Due to Intracranial Pressure. *Investigative Ophthalmology, Visual Science.* **57** (4), 1901–1911 (2016).

55. Downs, J. C. Optic nerve head biomechanics in aging and disease. *Experimental Eye Research.* **133**, 19–29 (2015).

56. Downs, J. C., Roberts, M. D., Burgoyne, C. F. Mechanical environment of the optic nerve head in glaucoma. *Optometry and Vision Science.* **85** (6), 425–435 (2008).

57. Downs, J. C. et al. Viscoelastic characterization of peripapillary sclera: material properties by quadrant in rabbit and monkey eyes. *Journal of Biomechanical Engineering.* **125** (1), 124–131 (2003).

58. Wagner, A. H. et al. Exon-level expression profiling of ocular tissues. *Experimental Eye Research.* **111**, 105–111 (2013).

59. Pels, E., Beele, H., Claerhout, I. Eye bank issues: II. Preservation techniques: warm versus cold storage. *International Ophthalmology.* **28** (3), 155–163 (2008).

60. Reinhard, K. et al. Hypothermia Promotes Survival of Ischemic Retinal Ganglion Cells. *Investigative Ophthalmology, Visual Science.* **57** (2), 658–663 (2016).